# Global Satellite Observations of Negative Brightness Temperature Differences between 11 and 6.7 $\mu$m

STEVEN A. ACKERMAN

*Cooperative Institute for Meteorological Satellite Studies, Space Science and Engineering Center, University of Wisconsin—Madison, Madison, Wisconsin*

(Manuscript received 16 October 1995, in final form 5 March 1996)

ABSTRACT

Global analyses of satellite spectral observations indicate the existence of negative brightness temperature differences between 11 and 6.7 $\mu$m ($BT_{11} - BT_{6.7}$) when cold scenes are viewed. Differences are typically greater than $-5$ K for the Tropics and midlatitudes but can be smaller than $-15$ K over high-altitude polar regions during winter. In July, more than 60% of the observations over the Antarctic Plateau had $BT_{11} - BT_{6.7} < -5$ K. In January, over Greenland, the frequency of occurrence is approximately 20%.

Three factors are investigated that may contribute to these observed negative brightness temperature differences: 1) calibration errors, 2) nonuniform scenes within the field of view, and 3) physical properties of the observed phenomena. Calibration errors and nonuniform scenes may generate values of $BT_{11} - BT_{6.7}$ that are less than zero; however, these differences are on the order of $-2$ K and, therefore, cannot fully explain the observations.

A doubling and adding radiative transfer model is used to investigate the physical explanations of the negative differences. Simulations of satellite spectral observations for thick clouds produce negative differences that are comparable to those observed in the Tropics and midlatitudes. The magnitude of the differences is a function of cloud microphysics, cloud-top pressure, view angle, and the cloud optical thickness. The model simulations are also capable of producing large negative differences over high-altitude polar regions.

Distinguishing clear and cloudy regions from satellite infrared radiances is a challenging problem in polar winter conditions. Brightness temperature differences between 11 and 6.7 $\mu$m provide a technique to separate cold, optically thick clouds from clear-sky conditions when strong radiation inversions exist at the surface. The presence of a cloud inhibits the development of this inversion and shields its detection using satellite radiance measurements. While physically reasonable, and in agreement with radiative transfer calculations, this technique has not been verified with ground nor with aircraft observations. Further evidence that the large negative values of $BT_{11} - BT_{6.7}$ are associated with surface inversions is presented by comparing the satellite observations with surface temperature measurements from an Antarctica automated weather station.

## 1. Introduction

Radiance measurements from satellites are now routinely used to monitor global climate parameters. Global analysis of cloud amounts, types, and optical properties using satellite measurements have been developed and are currently operational, for example, the International Satellite Cloud Climatology Project (Rossow et al. 1988; Rossow and Garder 1993) and $CO_2$ slicing; (Wylie et al. 1994). Frey et al. (1995) developed an end-to-end algorithm that performs collocation and analysis of High-Resolution Infrared Sounder/2 (HIRS/2) and Advanced Very High Resolution Radiometer (AVHRR) observations. This algorithm, referred to as Collocated HIRS/2 and AVHRR Products (CHAPS), was designed to operate on global observations and in a real-time, hands-off operational mode. Normally (see section 2), the 11-$\mu$m brightness temperature is greater than the 6.7-$\mu$m brightness temperature; however, the CHAPS data indicates a large frequency of occurrence in which the 6.7-$\mu$m brightness temperature is greater than the 11-$\mu$m brightness temperature. This paper discusses the nature of these negative differences and provides explanations for their existence.

Section 2 presents the observations of negative brightness temperature differences over high-altitude, snow-covered regions during night and over tropical clouds with cold cloud tops. Section 3 explores these negative differences with radiative transfer calculations. The results are summarized in section 4.

## 2. Observations of negative brightness temperature differences between 11 and 6.7 $\mu$m

The database used in this study consists of collocated observations from the AVHRR, the HIRS/2 radiance measurements (both on the NOAA satellites), and Na-

*Corresponding author address:* Dr. Steven A. Ackerman, Cooperative Inst. for Meteor. Satellite Studies, Space Science and Engineering Center, University of Wisconsin—Madison, 1225 West Dayton Street, Madison, WI 53706.
E-mail: stevea@ssec.wisc.edo

tional Centers for Environmental Prediction (NCEP) analysis fields. This collocation was accomplished by a global cloud-retrieval algorithm using the operational National Oceanic and Atmospheric Administration (NOAA) meteorological polar orbiting satellites. The CHAPS algorithm was run in real-time mode during July 1993 and 1994 and January 1994 using observations made from the *NOAA-12* spacecraft. The *NOAA-12* satellite is in an approximately 102-min sun-synchronous orbit with local observations made near 0730 and 1930 LST for most latitudes, but with more frequent sampling in the polar regions.

Discrimination between cloudy and clear scenes is essential to deriving accurate cloud products such as distributions of cloud altitude, cloud amount, and spectral cloud radiative forcing. The CHAPS clear-sky detection algorithm is presented in Frey et al. (1995). These global, coincident observations from the AVHRR and the HIRS/2 provide a database to explore potential differences in the radiative characteristics of clouds in different regions of the world at different times of the year. This paper focuses on HIRS/2 observations of channels 8 (11 $\mu$m) and 12 (6.7 $\mu$m).

In clear-sky situations, the 6.7-$\mu$m radiation measured by satellite instruments is emitted by water vapor in the atmospheric layer between approximately 200 and 500 hPa (Soden and Bretherton 1993; Wu et al. 1993) and has a brightness temperature ($BT_{6.7}$) related to the temperature and moisture in that layer. The 6.7-$\mu$m radiation emitted by the surface or low clouds is absorbed in the atmosphere and is not sensed by the satellite instruments. On the other hand, absorption by atmospheric gases is weak at 11 $\mu$m. Under clear-sky conditions, the measured 11-$\mu$m radiation originates primarily at the surface, with a small contribution by the near-surface atmosphere. The region between 200 and 500 hPa is not sensed at 11 $\mu$m. Because the surface is normally warmer than the upper troposphere, 11-$\mu$m brightness temperature $BT_{11}$ is normally warmer than 6.7-$\mu$m brightness temperature $BT_{6.7}$; thus, the difference, $BT_{11} - BT_{6.7}$, is normally greater than zero. The CHAPS global analyses of $BT_{11} - BT_{6.7}$ show large negative differences (less than $-10$ K) over the Antarctic Plateau and Greenland during their respective winters. Large negative differences may be indicative of clear-sky conditions and the existence of a strong low-level temperature inversions.

Figure 1 depicts the frequency of occurrence of HIRS/2 observations of $-5 \leq (BT_{11} - BT_{6.7}) \leq 0$ (Fig. 1a) and $(BT_{11} - BT_{6.7}) < -5$ (Fig. 1b) for July 1993 centered over the South Pole on a 2.5° × 2.5° latitude–longitude grid. Over the East Antarctica highlands, 60% of the observations showed large negative differences (less than $-5$ K). The sharp boundary in the frequency of occurrence between east and west Antarctica is a result of the Transantarctica Mountains.

Figure 2 shows a frequency of occurrence of negative $BT_{11} - BT_{6.7}$ observed over the Arctic in January 1994. Figure 2a is of $0 \geq (BT_{11} - BT_{6.7}) \geq -5$ and Fig. 2b represents the number of occurrences of $(BT_{11} - BT_{6.7}) < -5$. More than 15% of the observations over the Greenland plateau have $BT_{11} - BT_{6.7} < -5$. Other regions of large frequency of occurrence include Siberia and the Canadian Northwest Territory. Figures 1 and 2 display a distinct bias toward land in the occurrence of negative brightness temperature differences.

In polar regions, strong surface radiation inversions can develop as a result of longwave energy loss at the surface due to clear skies and a dry atmosphere. Figure 3 is a temperature (solid line) and dewpoint temperature (dashed line) profile measured over the South Pole at 0000 UTC on 13 September 1995 and illustrates this surface inversion. On this day, the temperature inversion was approximately 20 K over the lowest 100 m of the atmosphere. The surface temperature was more than 25 K colder than the temperature at 600 hPa. Temperatures over Antarctica near the surface can reach 200 K (Stearns et al. 1993), while the middle troposphere is 235 K. Under such conditions, satellite channels located in strong water vapor absorption bands, such as the 6.7-$\mu$m channel, will have a warmer equivalent brightness temperature than the 11-$\mu$m window channel. This brightness temperature difference between 11 and 6.7 $\mu$m may be very useful for detecting cloud-free conditions in the polar night. A doubling/adding model of the azimuthally averaged form of the infrared radiative transfer equation was used to simulate the brightness temperature differences at 11 and 6.7 $\mu$m using the temperature and moisture profile of Fig. 3, and a spectrally varying surface emissivity (Warren 1982; Salisbury and D'Aria 1992). The simulated $BT_{11} - BT_{6.7}$ difference was $-14$ K.

As indicated in Fig. 1, over the East Antarctica highlands, 60% of the observations showed large negative differences. Strong radiative cooling to the east of the Transantarctica Mountains is an important ingredient in the development of the katabatic winds that flow down through these mountains (Swithinbank 1973; Bromwich 1989; Breckenridge et al. 1993). Satellite observations of $BT_{11} - BT_{6.7}$ for winter highlands may aid in monitoring the development of this strong nocturnal inversion.

A box-plot (Tukey 1977) of the $BT_{11} - BT_{6.7}$ observations versus $BT_{11}$ observations, over intervals of 1 K, over the South Pole region in July 1993 is shown in Fig. 4. In this box-plot the squares represent median values and the rectangles denote the 75% and 25% quartiles. The whiskers represent the nonoutlier maximum and minimum defined mathematically as the maximum and minimum observed values that lie within the range

$$q_{25} - 1.5\, q_{\text{range}} > \text{Observation} < q_{75} + 1.5\, q_{\text{range}},$$

where $q_{25}$ and $q_{75}$ represent the 25% and 75% quartiles and $q_{\text{range}} = q_{75} - q_{25}$ is the interquartile range. Extreme values (asterisks) are cases satisfying

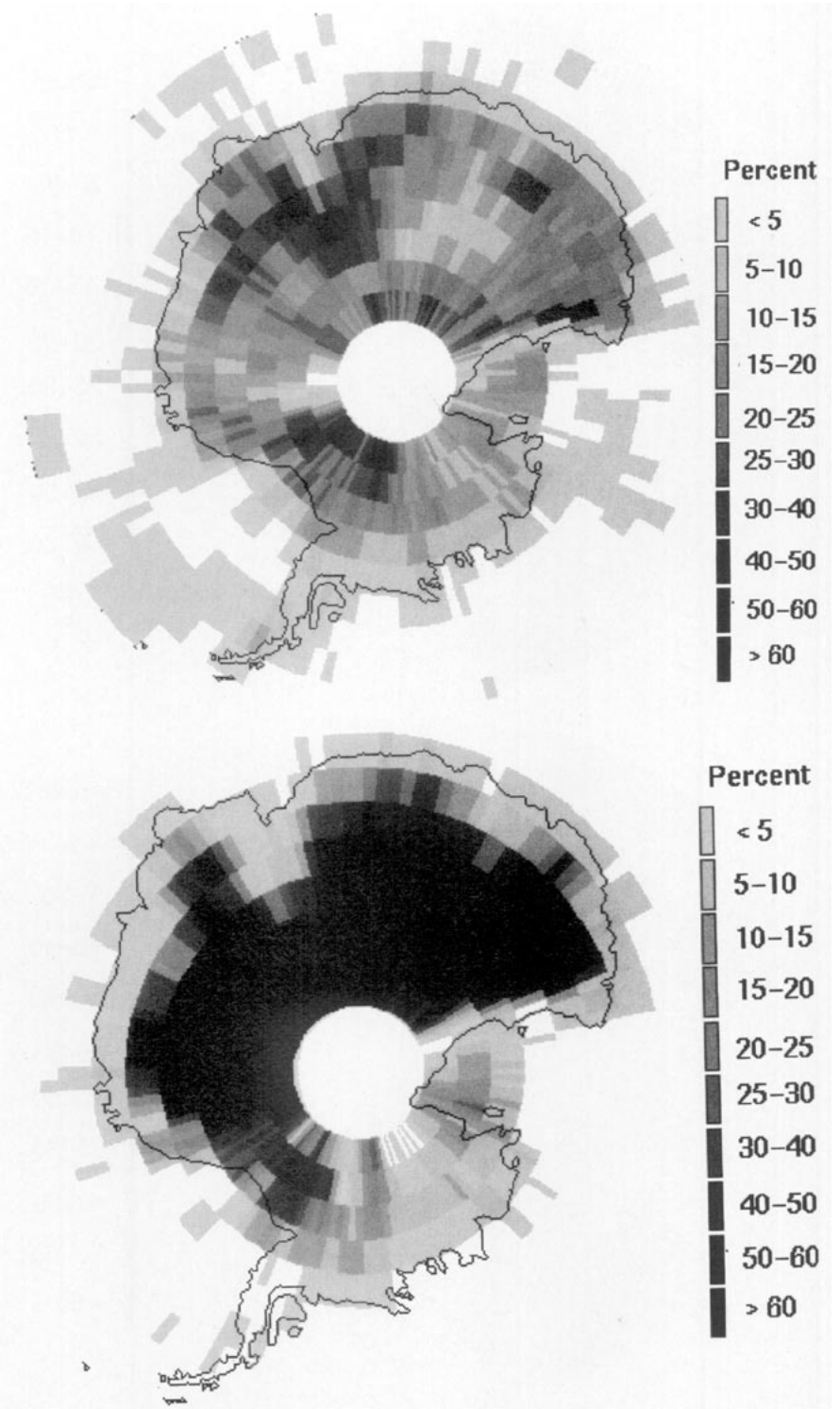


FIG. 1. Frequency of occurrence, in a 2.5° × 2.5° latitude–longitude grid, of HIRS/2 observations of (a) $0 \geq (BT_{11} - BT_{6.7}) \geq -5$ and (b) $(BT_{11} - BT_{6.7}) < -5$ for July 1993 over the South Pole. Percentages are listed in the legend.

$$q_{25} - 3.0\, q_{\text{range}} < \text{Observation} > q_{75} + 3.0\, q_{\text{range}}.$$

Outliers (circles) are denoted for those observations that are not extreme values and satisfy

$$q_{25} - 1.5\, q_{\text{range}} < \text{Observation} > q_{75} + 1.5\, q_{\text{range}}.$$

See Fig. 5 for a summary of the box-plot legend. As $BT_{11}$ gets colder, there is a decreasing trend in the me-

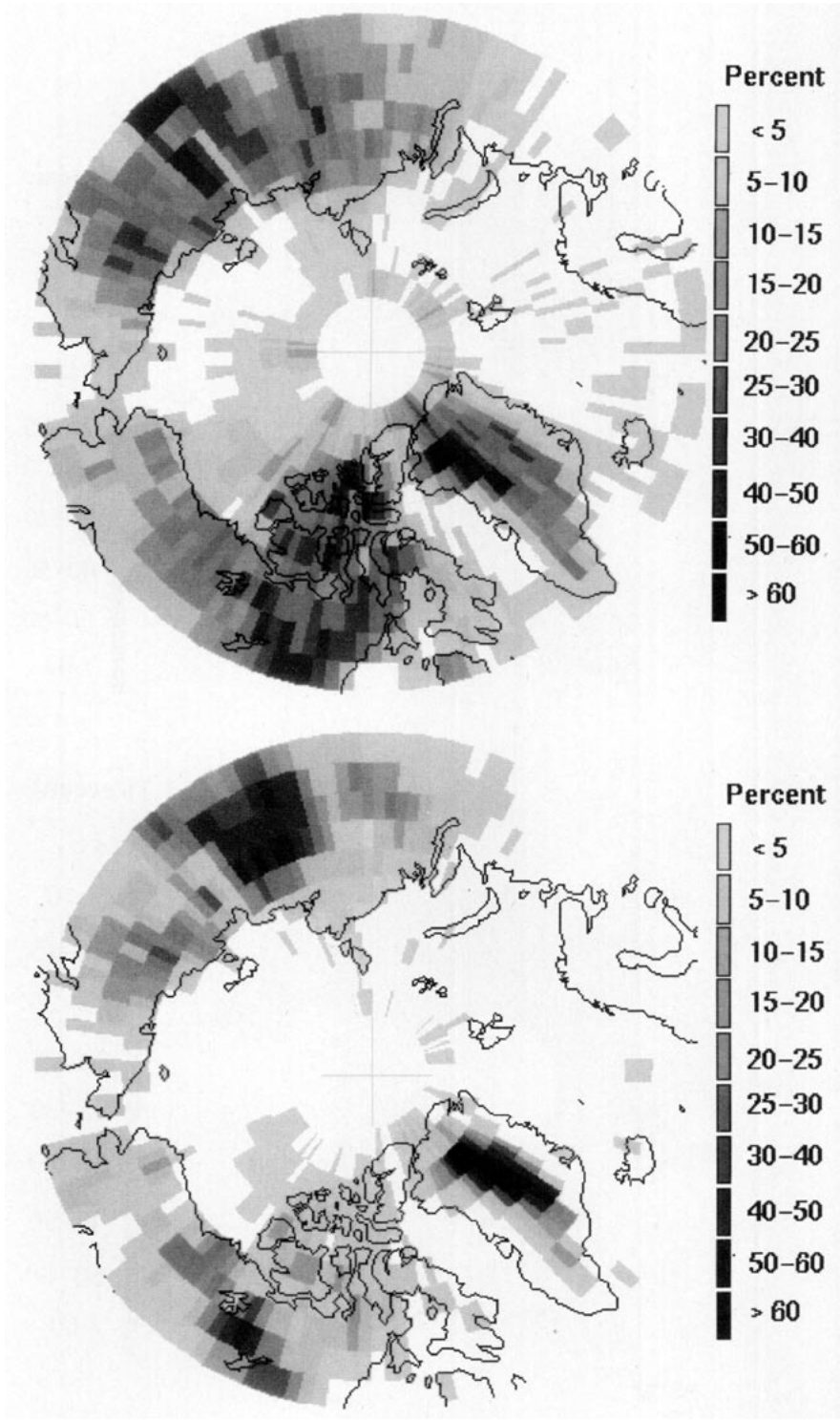


FIG. 2. As in Fig. 1 but for January 1994 over the North Pole.

dian value of $BT_{11} - BT_{6.7}$. Note the number of outliers and extreme values that occur for $BT_{11}$ greater than 230 K. These outliers, which occur for the more negative values of $BT_{11} - BT_{6.7}$, could result from the presence of a thin cirrus overlying a strong surface inversion. The impact of thin cirrus on the negative brightness temperature differences is addressed in section 2.4. In the $BT_{11}$ range 200 K to 210 K there are outliers of positive values of $BT_{11} - BT_{6.7}$. These outliers and extreme values are similar to the differences observed

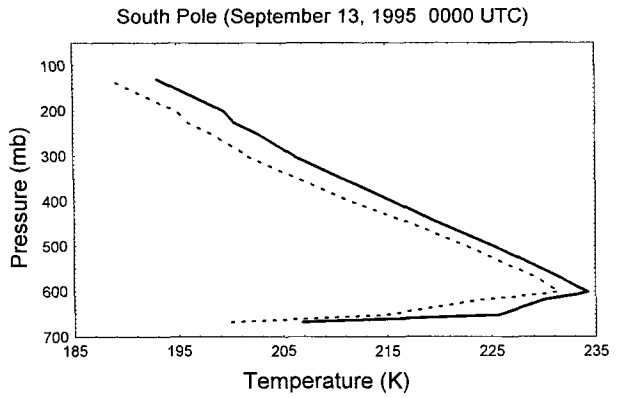


FIG. 3. Temperature (solid line) and dewpoint temperature (dashed line) measured over the South Pole at 0000 UTC 13 September 1995.

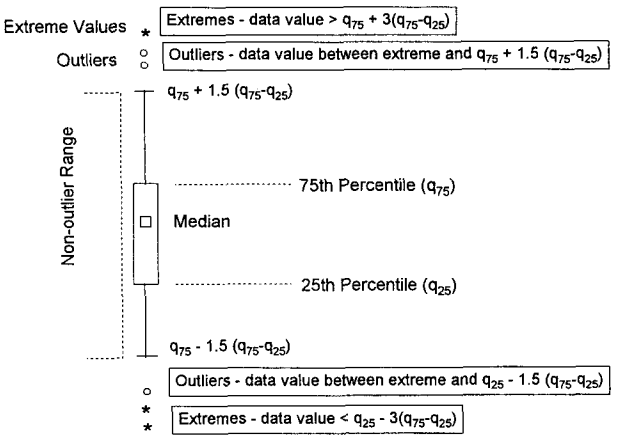


FIG. 5. Schematic diagram of a box-plot.

over tropical cold clouds, whose temperatures are similar to the clear-sky polar conditions discussed above.

Figure 6 depicts the frequency of occurrence of $-5 < BT_{11} - BT_{6.7} < 0$ within 50° of the equator, binned in a 2.5° lat × 2.5° long geographic grid, during January 1994 and July 1993. Unlike the polar winter cases, there are few values of $(BT_{11} - BT_{6.7}) < -5$. The occurrences of negative differences correlate highly with expected regions of convection. The intertropical convergence zone is apparent in both months, as is the shift in its position to the summer hemisphere. The summertime peak in convection over South America and convection associated with the southwest summer monsoon are also clearly visible in this figure. In addition, negative differences also appear in the midlatitude storm tracks of the winter hemisphere.

There are three factors that may contribute to these observed negative brightness temperature differences: 1) calibration errors, 2) nonuniform scenes within the field of view, and 3) physical properties of the observed phenomena. Each of these factors is discussed below.

### *a. Calibration errors*

The HIRS/2 instrument uses a rotating mirror to scan the earth by stepping at 1.8° intervals. To cover the 2240-km cross-track scan requires 56 steps of the mirror. The HIRS/2 enters calibration mode after 37 scans of the earth. Calibration is achieved by viewing space and a warm reference target (Lutz et al. 1990). The noise equivalent differential radiances (NE$\Delta$N) of the 11- and 6.7-$\mu$m channels are approximately 0.10 and 0.19 mW m$^{-2}$ str$^{-1}$ cm$^{-1}$, respectively. Error analysis conducted by Wu et al. (1993) suggests NE$\Delta$T of individual observations of $\pm$0.2 K and $\pm$0.92 K in the $BT_{11}$ and $BT_{6.7}$ observations, respectively. While ab-

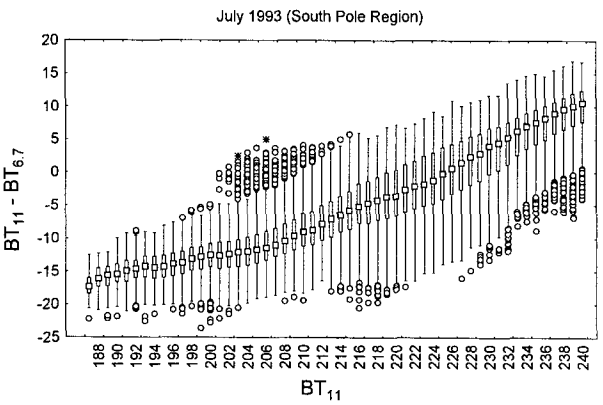


FIG. 4. Box-plot of the negative $BT_{11} - BT_{6.7}$ observations versus $BT_{11}$ observations, over intervals of 1 K, over the South Pole region in July 1993. Squares represent median values, and rectangles denote the 75% and 25% quartiles. The whiskers represent the nonoutlier maximum and minimum. Outliers and extreme values are denoted by circles and asterisks, respectively. See Fig. 5 for a schematic representation.

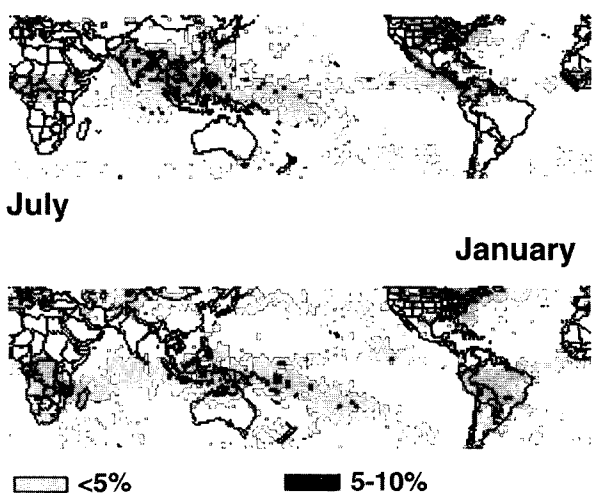


FIG. 6. Frequency of occurrence of $-5 < BT_{11} - BT_{6.7} < 0$ within 50° of the equator, binned in a 2.5° lat × 2.5° long geographic grid, during January 1994 and July 1993.

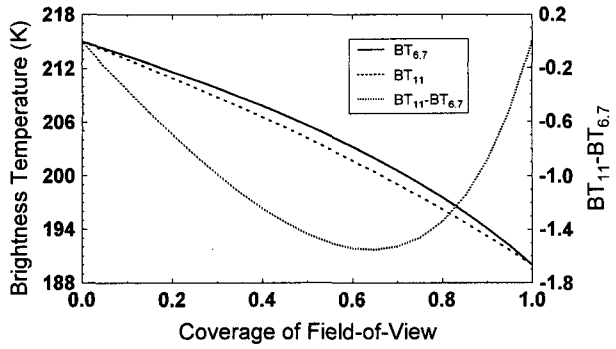


FIG. 7. Effect of cloud variability in the FOV on the brightness temperatures of 11 and 6.7 $\mu$m. Two clouds in the FOV are assumed, one with a temperature of 190 K and the second with a temperature of 215 K. Here, $f$ represents the 190-K cloud fraction. The solid and dashed lines represent the $BT_{6.7}$ and $BT_{11}$ observations as a function of $f$. The difference between the two brightness temperatures is the dotted line whose scale is the right-hand ordinate.

solute calibration errors can contribute to negative $BT_{11} - BT_{6.7}$ observations, such errors cannot generate the $-5$ K differences shown in Figs. 1b and 2b.

### b. *Nonuniform fields of view*

The HIRS/2 instantaneous field of view (IFOV) is approximately 18 km in diameter at nadir and approximately 58 km cross-track by 30 km along-track at the end of the scan. CHAPS limits its analysis to $\pm 30°$ of nadir. As the Planck function is nonlinear, a nonuniform IFOV composed of two blackbodies with different temperatures can generate a spectral brightness temperature difference if the spectral channels are widely spaced. Consider an IFOV containing a scene with two clouds, one with a temperature of 190 K and the other at a temperature of 215 K. Assuming the clouds behave as blackbodies, the observed radiance is estimated by linearly averaging the radiance at each of these temperatures as a function of the fraction of cloud cover within the IFOV; that is

$$I^{\lambda}_{\text{measured}} = fI^{\lambda}_{190} + (1 - f)I^{\lambda}_{215},$$

where $I^{\lambda}_{190}$ and $I^{\lambda}_{215}$ are the radiance at 190 K and 215 K, respectively; at wavelength $\lambda$, $f$ is the fraction of the field of view covered by the cloud with a temperature of 190 K; and $I^{\lambda}_{\text{measured}}$ is the measured radiance of the nonhomogeneous IFOV. The measured radiance is then converted to a brightness temperature and the result shown in Fig. 7. The solid and dashed lines represent the $BT_{6.7}$ and $BT_{11}$ observations as a function of $f$. The difference is the dotted line whose magnitude is noted on the right-hand ordinate. It is possible to generate a $BT_{11} - BT_{6.7}$ difference of $-1.5$ K based on scene nonuniformity; however, some of the observed differences over tropical convection are less than $-3$ K and in the case of polar winter scenes less than $-15$ K.

### c. *Physical properties of the observed phenomena*

Absolute calibration errors and nonuniform FOVs do not exclude a natural cause for the observed negative $BT_{11} - BT_{6.7}$ quantities. Figure 8 is a box-plot of the brightness temperature difference versus $BT_{11}$ for observations made in January 1994 and July 1993 and bounded by 50°N and 50°S latitudes. The relationship between the median value of $BT_{11} - BT_{6.7}$ versus $BT_{11}$ is similar for the two months. January displays greater variability about this relationship, particularly in the nonoutlier maximum and minimum values. For $BT_{11}$ less than approximately 206 K, the median values of $BT_{11} - BT_{6.7}$ are negative and, except for the few values of $BT_{11} = 186$ K, remain negative. Over this geographic region there are very few values of $BT_{11} - BT_{6.7} < -5$. The extreme values and outliers observed for $BT_{11} < 200$K over the Antarctic (Fig. 4) are uncommon observations in the tropical convective regions of the earth. This suggests that the extreme and outlying values of Fig. 4 are thick, cold clouds. This is supported by a scatter diagram of $BT_{11} - BT_{6.7}$ versus $BT_{11}$ (not shown) for the two geographic regions. Thus, at cold temperatures in the polar regions, the $BT_{11} - BT_{6.7}$ versus $BT_{11}$ analysis may distinguish

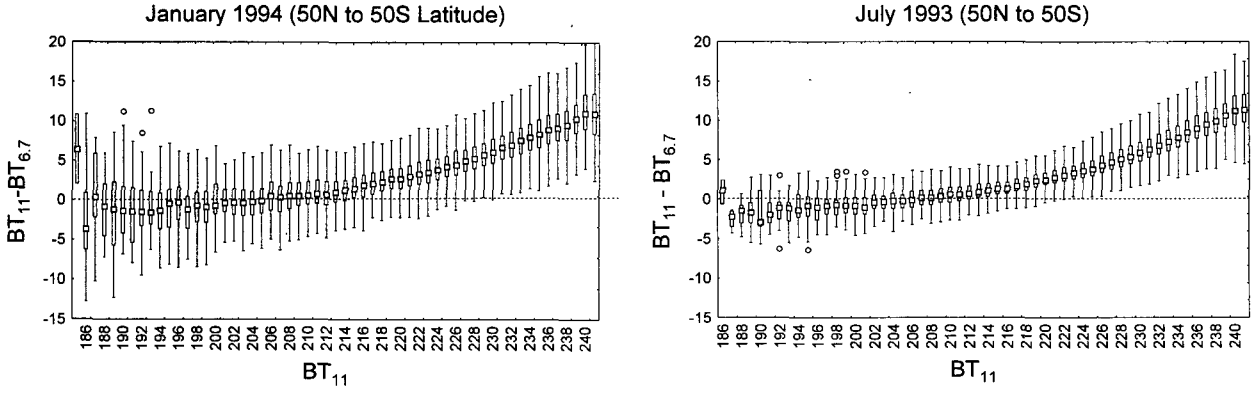


FIG. 8. Box-plot of the negative $BT_{11} - BT_{6.7}$ observations versus $BT_{11}$ observations, over intervals of 1 K, observed in (a) January 1994 and (b) July 1993 for measurements bounded by 50°N and 50°S latitudes.

clear-sky inversion cases from cold clouds. This is investigated in the following section using theoretical simulations.

### d. *Simulations of differences over strong nocturnal inversions*

The large negative differences of $BT_{11} - BT_{6.7}$ observed over the polar high-altitude plateaus in winter are consistent with theory and physical expectations. Detecting the presence of this surface inversion is important, as the energy exchanges at a snow–ice surface are dominated by radiative processes (Maykut 1986; Gow and Tucker 1990). During winter conditions, the magnitude of the longwave net radiation balance is largely driven by the presence or absence of clouds. For cloud-free conditions, the net infrared flux is large and is directed away from the surface, thus causing the cooling of the lower layers of the atmospheres. This radiative cooling plays an important role in the formation of cold air masses, which may develop into downslope winds (foehns and boras).

In this section, model simulations were used to investigate if the negative brightness temperature difference can be observed in the presence of cirrus clouds. The temperature and moisture profiles of Fig. 3 were used in a sensitivity analysis. The effects of the presence of high cloud on the simulated satellite observed radiances were investigated assuming cirrus clouds situated between 250 and 300 hPa.

This sensitivity analysis was performed using the azimuthally averaged form of the infrared radiative transfer equation:

$$\mu \frac{dI(\tau, \mu)}{d\tau} = I(\tau, \mu) - (1 - \omega_0)B(T) - \frac{\omega_0}{2}\int_{-1}^{1} P(\tau, \mu, \mu')I(\tau, \mu')\, d\mu', \quad (1)$$

where $B(T)$ is the Planck function at temperature $T$, $\omega_0$ is the single scattering albedo, $P(\tau, \mu, \mu')$ is the phase function, and $\tau$ is optical depth. The radiative transfer equation was solved using a doubling and adding model with a spectral resolution of 20 $cm^{-1}$. Spectral absorption by gases was assigned according to Stackhouse and Stephens (1991). As this study aims to assess the potential impact of clouds obscuring the temperature inversion, Mie theory was used to calculate the single scattering properties of the cloud. The particle-size distribution was assumed to follow a gamma distribution with an effective radius of 12 $\mu$m. The surface IR spectral reflectance follows that of Warren (1982) and Salisbury and D'Aria (1992) and was assumed to be independent of angle. If no cloud is present, the $BT_{11} - BT_{6.7}$ difference is $-14$ K. Varying the surface spectral emissivity changes the difference by approximately $\pm 0.5$ K. Figure 9 depicts the theoretical simulation of $BT_{11} - BT_{6.7}$ versus cloud ice water path (IWP) for a nadir view. This simulation indicates that clouds with an IWP of greater than approximately 20 g $m^{-2}$ will obscure a surface temperature inversion, if one exists. For thick clouds, the brightness temperature differences are significantly less than those associated with nocturnal inversions. The sensitivity of $BT_{11} - BT_{6.7}$ to cloud microphysical and macrophysical properties is explored in section 2f.

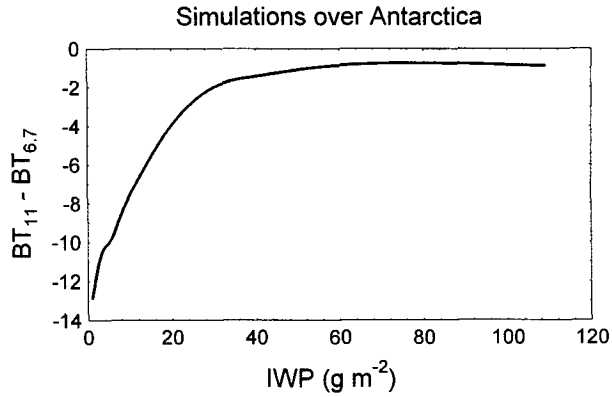


FIG. 9. Theoretical simulation of $BT_{11} - BT_{6.7}$ versus cloud ice water path for clouds overlying a strong nocturnal inversion typical of the Antarctic Plateau.

### e. *Comparison with surface meteorological observations*

The model simulations of the winter Antarctic atmosphere are consistent with the HIRS/2 observations. While these simulations are convincing, validation that the differences result from the presence of a temperature inversion requires additional measurements of the state of the atmosphere. Further evidence is presented by comparing the satellite observations with temperature measurements from an automated weather station (AWS). Stearns et al. (1993) discuss the instrumentation and data processing procedures of the Antarctic AWS measurements. Figure 10 compares the satellite measurements with the AWS observations for July 1993. The solid line is the 3-hourly averaged air temperature measured at Dome C (74.50°S, 123°E). The 30°C temperature range reflects changes in cloud conditions. The warmer air temperatures are a result of increased downward longwave radiative flux due to the presence of cloud (Sinkula 1993). The open circles represent the $BT_{11}$ measured by the HIRS/2 within a 0.5° latitude/longitude grid centered on Dome C. The satellite-measured brightness temperatures capture the daily changes in the temperature measured at Dome C. There are many instances during July 1993 when the $BT_{11}$ was less than the AWS-measured air temperature, indicating the existence of a surface temperature inversion. The larger the difference between the AWS air temperature and the $BT_{11}$, the steeper the surface temperature inversion. The filled circles in Fig. 10 represent observations of $BT_{11} - BT_{6.7}$, the scale of which

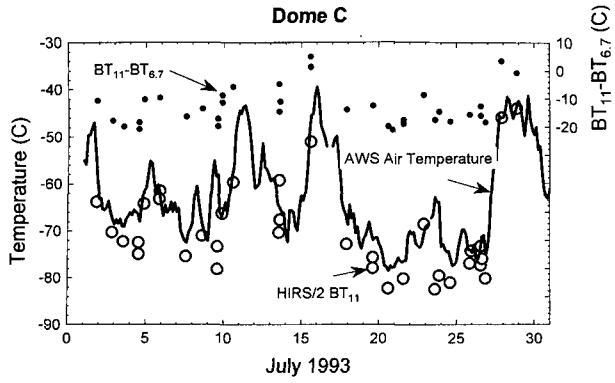


FIG. 10. Comparison of satellite measurements with the surface observations over Antarctica during July 1993. The solid line is the 3-hourly averaged air temperature measured at Dome C (74.50°S, 123°E). The open circles represent the $BT_{11}$ measured by the HIRS/2 within a 0.5° latitude/longitude grid centered on Dome C. The filled circles represent observations of $BT_{11} - BT_{6.7}$, the scale of which is on the right-hand axis.

is on the right-hand axis. For this location and month, $BT_{11} - BT_{6.7}$ less than −10°C occur when the AWS air temperature is less than −70°C, an indication of clear-sky conditions and the presence of surface radiation inversion (Sinkula 1993).

### *f. Simulations of differences over cold tropical clouds*

Observations at 11 and 6.7 $\mu$m have been used to study high clouds (e.g., Szejwach 1982; Pollinger and Wendling 1984; Liou et al. 1990). This section focuses on simulating the observed negative differences between the two spectral brightness temperatures. The $BT_{11}$ and $BT_{6.7}$ observations were simulated using the doubling/adding model discussed above. The gas distributions and temperature profile of a standard tropical atmosphere were assumed and an optically thick cloud (LWP of 40 g $m^{-2}$) was placed at various levels in the atmosphere. A range of effective particle radii was assumed along with different viewing angles consistent with the CHAPS observations (Frey et al. 1995). Figure 11 depicts the range of the simulated $BT_{11} - BT_{6.7}$ as a function of the $BT_{11}$ values. For cold clouds ($BT_{11} < 210$ K) negative values are produced, in good agreement with the observations (e.g., Fig. 8). Negative values arise due to nonlinearity of the Planck function and the presence of water vapor above the cloud tops. While the emissivity of the cloud is a function of particle size, the spectral differences in the emissivity between 6.7 and 11 $\mu$m are small; however, gray clouds will generate negative differences of several tenths of a degree due to the nonlinear relationship between the observed radiance and brightness temperature. In addition, the amount of radiation reflected at cloud top is greater at 6.7 $\mu$m due to the larger downward radiance incident on cloud top. As the cloud top is placed lower in the atmosphere, water vapor absorption above the cloud decreases the 6.7-$\mu$m radiance, with only a small effect on the 11-$\mu$m observations. Thus, the negative differences are reduced and eventually become positive, as in the clear sky condition. The range in $BT_{11} - BT_{6.7}$ for a given $BT_{11}$ results from varying cloud microphysical properties, view angles, and water vapor structure above the cloud top.

If a physical mechanism is responsible for the observed differences over cold clouds, then other satellite observations should also measure negative values of $BT_{11} - BT_{6.7}$. Negative values have also been observed with the *GOES-7* VAS [Visible Infrared Spin Scan Radiometer (VISSR) Atmospheric Sounder] in the Multi-Spectral Imaging (MSI) mode. Calibration of the VAS instrument is discussed by Menzel et al. (1981). Random noise of individual observations at a scene temperature of 230 K is ±1.2 K and ±0.3 K in the $BT_{6.7}$ and $BT_{11}$ observations, respectively (W. P. Menzel, personal communication, 1995). Eight cloud systems, including their environments, in the eastern tropical Pacific (10°S–20°N, 120°–150°W) between 1700 and 1900 UTC were sampled using the *GOES-7* VAS 11- and 6.7-$\mu$m channels during the fall of 1992. A histogram of $BT_{11} - BT_{6.7}$ values as measured by the VAS is given in Fig. 12. Negative values are observed by the VAS that are consistent with the HIRS/2 observations and theoretical simulations.

## 3. Summary

Global observations of cold scenes by the HIRS/2 demonstrate that valid 6.7-$\mu$m brightness temperature measurements may be greater than the corresponding window channel values. Similar observations were seen in a limited set of *GOES-7* VAS observations. At issue is the physical explanation of these observations and potential applications to remote sensing the environment.

Calibration errors and nonuniform fields of view are capable of generating negative values of $BT_{11} - BT_{6.7}$; however, the magnitude is not comparable to the ob-

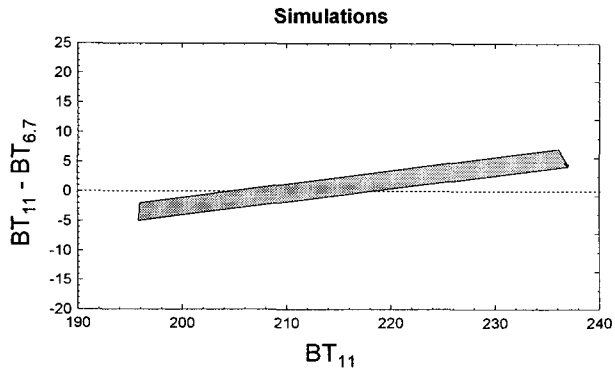


FIG. 11. Range of simulated $BT_{11} - BT_{6.7}$ as a function of $BT_{11}$ assuming a standard tropical atmosphere and various cloud types and viewing angles.

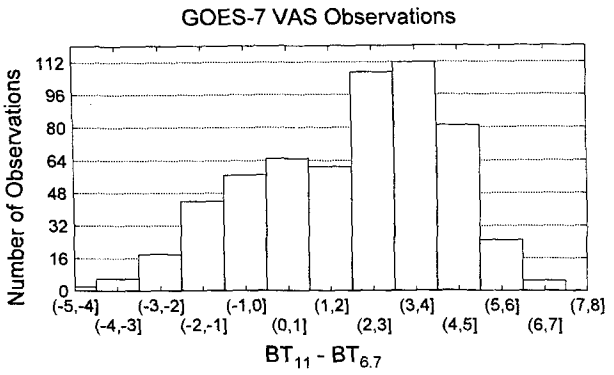


FIG. 12. Histogram of $BT_{11} - BT_{6.7}$ values as observed by the *GOES-7* VAS instrument.

servations reported here. Radiative transfer model studies indicate that the negative differences are a result of a strong surface temperature inversion or cold clouds high in the troposphere.

A doubling and adding radiative transfer model is used to investigate the physical explanations of the negative differences. Simulations of the satellite spectral observations for thick clouds produce negative differences that are comparable to those observed in the Tropics and midlatitudes. The magnitude of the differences are a function of cloud microphysics, cloud-top pressure, view angle, and the cloud optical thickness. The model simulations are also capable of producing large negative differences over high-altitude polar regions in the presence of a surface inversion.

The brightness temperature differences between 11 and 6.7 $\mu$m can be used to detect the existence of strong surface inversions. Clouds inhibit the formation of the inversion and obscure the inversion from satellite detection if the IWP is greater than approximately 20 g $m^{-2}$. In July, more than 60% of the observations over the Antarctic Plateau had $BT_{11} - BT_{6.7} < -5$ K. In January over Greenland, the frequency of occurrence is approximately 20%. Further evidence is presented by comparing the satellite observations with temperature measurements from an automated weather station (AWS) Dome C (74.50°S, 123°E). The satellite measured $BT_{11}$ captured the daily changes in the air temperature measured at Dome C. There were many instances during July 1993 when the $BT_{11}$ was less than the AWS measured air temperature, indicating the existence of a surface temperature inversion. For this location and month, $BT_{11} - BT_{6.7}$ less than $-10$°C occurred when the AWS air temperature is less than $-70$°C—a surface temperature indicative of clear-sky conditions and the presence of surface radiation inversion.

The analysis presented demonstrates that negative differences are also observed over high clouds with temperatures colder than approximately 210 K. There is, however, much scatter in the observations, and whether this variability is associated with specific cloud types and atmospheric conditions requires a more detailed analysis.

Clouds in the polar regions, where the cloud temperature is often nearly the same, or even warmer than the surface temperature, are difficult to detect using passive radiometric measurements from satellites. During the polar winter, cloud detection techniques must revert to infrared algorithms only, increasing the difficulties of detection. A method to distinguish clear-sky conditions over high-altitude polar regions during nighttime may be feasible using brightness temperature differences between 11-$\mu$m and 6.7-$\mu$m observations. This clear-sky detection method is based on the occurrence of strong surface radiative inversions that develop in winter conditions.

*Acknowledgments.* This work was supported by the NOAA Climate and Global Change Program under Grant NA26GP0234-01, the NASA FIRE Program under Grant NAS1-1177, and the NASA TRMM Grant NAG5-1586. The author is indebted to programming efforts of R. A. Frey and discussions with C. Moeller. A portion of this work was completed during the author's visit to the Institute of Atmospheric Physics, DLR, Germany.

## REFERENCES

Ackerman, S. A., W. L. Smith, J. D. Spinhirne, and H. E. Revercomb, 1990: The 27–28 October 1986 FIRE IFO cirrus case study: Spectral properties of cirrus clouds in the 8–12 $\mu$m window. *Mon. Wea. Rev.*, **118,** 2377–2388.

Breckenridge, C. J., U. Radok, C. R. Stearns, and D. H. Bromwich, 1993: Katabatic winds along the transantarctic mountains. *Antarct. Meteor. Climatol.*, **61,** 69–92.

Bromwich, D. H., 1989: Satellite analyses of Antarctic katabatic wind behavior. *Bull. Amer. Meteor. Soc.*, **70,** 738–749.

Frey, R. A., S. A. Ackerman, and B. J. Soden, 1996: Climate parameters from satellite spectral measurements. Part I: Collocated AVHRR and HIRS/2 observations of spectral greenhouse parameter. *J. Climate,* **9,** 327–344.

Gow, A. J., and W. B. Tucker III, 1990: Sea ice in the polar regions. *Physical Science,* Vol. A, W. O. Smith Jr., Ed., *Polar Oceanography,* Academic Press, 47–122.

Liou, K. N., S. C. Ou, Y. Takano, F. P. J. Valero, and T. P. Ackerman, 1990: Remote sounding of the tropical cirrus cloud temperature and optical depth using 6.5 and 10.5 $\mu$m radiometers during STEP. *J. Appl. Meteor.*, **29,** 716–726.

Lutz, H. J., W. L. Smith, and E. Raschke, 1990: A note on the improvement of TIROS operational vertical sounder temperature retrievals above the Antarctic snow and ice fields. *J. Geophys. Res.*, **95,** 11 747–11 754.

Maykut, G. A., 1986: The surface heat and mass balance. *The Geophysics of Sea Ice,* N. Untersteiner, Ed., NATO ASI Series, Vol. 146, Plenum Press, 395–464.

Menzel, W. P., W. L. Smith, and L. D. Herman, 1981: Visible infrared spin-scan radiometer atmospheric sounder radiomteric calibration: An inflight evaluation from intercomparisons with HIRS and radiosonde measurements. *Appl. Opt.,* **20,** 3641–3644.

Pollinger, W., and P. Wendling, 1984: A bispectral method for the height determination of optically thin ice clouds. *Contrib. Atmos. Phys.*, **57,** 269–281.

Rossow, W. B., and L. C. Garder, 1993: Cloud detection using satellite measurements of infrared and visible radiances for ISCCP. *J. Climate,* **6,** 2341–2369.

——, ——, P. Lu, and A. Walker, 1988: International Satellite Cloud Climatology Project (ISCCP), documentation of cloud data. WMO/TD 266, 153 pp. [Available from WMO P.O. Box 5, CH1211 Geneva 20, Switzerland.]

Salisbury, J. W., and D. M. D'Aria, 1992: Emissivity of terrestrial material in the 8–14 $\mu$m atmospheric window. *Remote Sens. Environ.,* **42,** 83–106.

Sinkula, B., 1993: Application of AWS data for Antarctic operational forecasting and climatic research. M.S. thesis, Department of Atmospheric and Oceanic Sciences, University of Wisconsin—Madison, 177 pp. [Available from University of Wisconsin—Madison, Madison, WI 53706.]

Soden, B. J., and F. P. Bretherton, 1993: Upper tropospheric relative humidity from the GOES 6.7 $\mu$m channel: Method and climatology for July 1987. *J. Geophys. Res.,* **98,** 16 669–16 688.

Stackhouse, P. W., and G. L. Stephens, 1991: A theoretical and observational study of the radiative properties of cirrus: Results from FIRE 1986. *J. Atmos. Sci.,* **48,** 2044–2059.

Stearns, C. R., L. M. Keller, G. A. Weidner, and M. Sievers, 1993: Monthly mean climatic data for Antarctic automatic weather stations. *Antarct. Meteor. Climatol.,* **61,** 1–21.

Swithinbank, C., 1973: Higher resolution satellite pictures. *Polar Rec.,* **16,** 739–751.

Szejwach, G., 1982: Determination of semitransparent cirrus cloud temperature from infrared radiances: Application to METEOSAT. *J. Appl. Meteor.,* **21,** 384–393.

Tukey, J. W., 1977: *Exploratory Data Analysis.* Addison-Wesley, 688 pp.

Warren, S. G., 1982: Optical properties of snow. *Rev. Geophys. Space Phys.,* **20,** 67–89.

Wielicki, B. A., and Coauthors, 1990: The 27–28 October 1986 FIRE IFO cirrus case study: Comparison of radiative transfer theory with observations by satellite and aircraft. *Mon. Wea. Rev.,* **118,** 2356–2376.

Wu, X., J. J. Bates, and S. Singhkhalsa, 1993: A climatology of the water vapor band brightness temperatures for NOAA operational satellites. *J. Climate,* **6,** 1282–1300.

Wylie, D. P., W. P. Menzel, H. M. Woolf, and K. I. Strabala, 1994: Four years of global cirrus cloud statistics using HIRS. *J. Climate,* **7,** 1972–1986.